Water Research 142 (2018) 452–458

Contents lists available at ScienceDirect

Water Research

journal homepage: www.elsevier.com/locate/watres

Wavelength-dependent chlorine photolysis and subsequent radical production using UV-LEDs as light sources

Ran Yin [a], Li Ling [a, **], Chii Shang [a, b, *]

[a] Department of Civil and Environmental Engineering, The Hong Kong University of Science and Technology, Clear Water Bay, Kowloon, Hong Kong
[b] Hong Kong Branch of Chinese National Engineering Research Center for Control & Treatment of Heavy Metal Pollution, The Hong Kong University of Science and Technology, Clear Water Bay, Kowloon, Hong Kong

ARTICLE INFO

Article history:
Received 25 January 2018
Received in revised form
3 June 2018
Accepted 8 June 2018
Available online 14 June 2018

Keywords:
UV-LED
Wavelength-dependency
Chlorine photodecay
Radical formation
Model

ABSTRACT

UV-LEDs are considered as the most promising UV light sources, because it has the potential to replace conventional UV lamps in some water treatment applications in the foreseeable future. In this study, UV-LEDs at four wavelengths in the UV-C or near UV-C range (i.e., 257.7, 268, 282.3, and 301.2 nm) were used to investigate the wavelength-dependency on chlorine photolysis and its subsequent radical formation. The fluence-based photodecay rates of hypochlorous acid (HOCl) and hypochlorite (OCl^-) were monotonically correlated to their molar absorption coefficients and quantum yields, and the chlorine photodecay rates were much more significantly affected by molar absorption coefficients ($\beta = 0.949$) than quantum yields ($\beta = 0.055$). An empirical model that incorporated the chlorine photodecay rate constants, quantum yields, and molar absorption coefficients of HOCl and OCl^- was established, validated and then used to predict the chlorine photodecay rate at any wavelength (257.7–301.2 nm) and pH (5–10). The modelling results suggested that the maximum fluence-based rate constant ($1.46 \times 10^{-4}\ m^2\ J^{-1}$) was obtained at 289.7 nm and pH 9.95. The wavelength dependency was larger at alkaline pH than at acidic pH, and the pH dependency was the largest at the longest wavelength. The formation of hydroxyl radicals (HO·) and reactive chlorine species (RCS) decreased with increasing wavelength at pH 6, and increased with increasing wavelength at pH 7. More HO· was formed at pH 6 than pH 7, but RCS showed the opposite pH-dependency. The findings in this study provide the fundamental information in selecting UV-LEDs with specific wavelength for enhancing/optimizing chlorine photodecay and/or its radical generation at different pHs in real-world applications.

1. Introduction

Photolysis of chlorine by ultraviolet (UV) radiation (or sunlight) occurs in a number of water treatment scenarios. The photo-dechlorination by UV-C radiation has been used in some recreational waters (e.g., swimming pool water) and drinking water containing residual chlorine at households or residential buildings (Cassan et al., 2006; Weng et al., 2012). The degradation of chlorine in a multiple-barrier disinfection system is also important. Chlorine residuals, from the pre-oxidation process in the multiple-barrier disinfection system, will absorb UV light and decrease the UV disinfection efficiency by competing photons that are intended for inactivating chlorine-resistant pathogens (e.g., Cryptosporidium and Giardia) (Kashinkunti et al., 2004; Örmeci et al., 2005; Forsyth et al., 2013; Zhou et al., 2014). Therefore, the photo-dechlorination can enhance the overall disinfection efficiency of a multiple-barrier disinfection system (Kashinkunti et al., 2004). A better understanding of the chlorine photodecay could prevent the swimmers or citizens from exposure to chlorine-ordinated contaminants, and help design and implement a better multiple-barrier disinfection system.

UV-C can also activate chemical oxidants, including peroxide and chlorine, to produce radical species for the destruction of organic contaminants. The UV/peroxide advanced oxidation process (AOP), which produces hydroxyl radicals (HO·) through photolysis of peroxide at 254 nm using conventional UV mercury

* Corresponding author. Department of Civil and Environmental Engineering, The Hong Kong University of Science and Technology, Clear Water Bay, Kowloon, Hong Kong.
** Corresponding author. Department of Civil and Environmental Engineering, The Hong Kong University of Science and Technology, Clear Water Bay, Kowloon, Hong Kong.
E-mail address: cechii@ust.hk (C. Shang).

https://doi.org/10.1016/j.watres.2018.06.018
0043-1354/

lamps, is a common strategy for micropollutant abatement in drinking water treatment and potable water reuse (Rosenfeldt and Linden, 2007). However, the process is often hindered by its high-energy demand, due to low absorbance and low quantum yields of peroxide at 254 nm, as well as the presence of HO· scavengers (e.g., natural organic matter and bicarbonate) in real water (He et al., 2012; Wang et al., 2000). The UV/chlorine AOP based on the photolysis of free chlorine using conventional UV mercury lamps (low-pressure and medium-pressure UV lamps) is an alternative to the UV/peroxide AOP for degrading micropollutants in drinking water treatment and potable water reuse (Jin et al., 2011; Remucal and Manley, 2016; Deng et al., 2014; Dotson et al., 2012). It produces a more diverse spectrum of reactive species including reactive oxygen species (e.g., ozone and HO·) and reactive chlorine species (RCS), which complement each other in the contaminant degradation (Fang et al., 2014; Remucal and Manley, 2016; Sun et al., 2016; Watts and Linden, 2007; Yang et al., 2016). It is also more energy efficient and gives higher HO· yields than the UV/peroxide AOP at pH 6–7, due to the higher molar absorbance and quantum yields of hypochlorous acid (HOCl) compared to hydrogen peroxide (Stefan, 2017; Fang et al., 2014; Yin et al., 2018).

One drawback of the UV-based dechlorination and AOPs is the use of UV mercury lamps (low-pressure, medium-pressure and high-pressure UV lamps). Conventional UV mercury lamps have short lifespans, contain toxic mercury, and are fragile and oversized (Song et al., 2016). UV light emitting diodes (UV-LEDs), which are mercury-free, robust, compact and can turn on and off instantly, are potential alternatives and regarded as promising UV light sources (Chen et al., 2017; Würtele et al., 2011). By 2020, the wall plug efficiency and lifetimes of UV-LEDs are predicted to increase to more than 75% and 20,000 h, respectively, with a price drop by 40% (Song et al., 2016). More interestingly, UV-LEDs provide versatility in emitting light at any designated wavelength. For example, UV-LEDs make it possible to provide UV-C light at 200–300 nm (Muramoto et al., 2014) and, at this moment, UVC-LEDs at 255, 265 and 285 nm are commonly available in the market (Chen et al., 2017; Muramoto et al., 2014) We anticipate that such versatility facilitates easy matching of their emission spectra with the absorption and/or quantum yield maxima of free chlorine to enhance its photoreaction. However, this hypothesis has not been verified, and the fundamentals of this wavelength overlap phenomenon with respect to chlorine photo-reaction have not yet been established.

HOCl and OCl^- have wide absorption spectra that peak at 235 nm and 292 nm, with molar absorption coefficients of 101 M^{-1} cm^{-1} and 365 M^{-1} cm^{-1}, respectively (Feng et al., 2007). However, due to the limited availability of UV light sources, the chlorine photolysis and their quantum yields have only been examined at the wavelengths of 254 nm (UV-C), 303–313 nm (UV-B), 355–365 nm (UV-A) and 200–400 nm (MPUV) (Buxton et al., 1988; Remucal and Manley, 2016; Stefan, 2017). These wavelengths can hardly match the highest absorption spectra of free chlorine to unleash the highest rate of the chlorine photolysis. None of these wavelengths matches the wavelengths of UVC-LEDs, which are more energy efficient with increasing wavelength from 255 to 285 nm, in the present market. Moreover, there has not been any protocol/model established to predict the chlorine photolysis at different wavelengths, not to mention to select appropriate wavelengths of UV light for chlorine photolysis. The knowledge gap also exists in the wavelength-dependency on the production of reactive species from chlorine photolysis and its relationship with the chlorine photodecay. The chlorine photolysis produces HO· and Cl· at wavelengths shorter than 300 nm, but information on the HO· yield is only available at 254, 303–313 nm (UV-B), and 200–400 nm (MPUV) (Remucal and Manley, 2016; Stefan, 2017). And the wavelength-dependency on the formation of reactive chlorine species (e.g., Cl·, ClO· and $Cl_2^{\cdot-}$) remains unknown.

This study investigated the wavelength dependency on chlorine photolysis and the subsequent radical generation at four different wavelengths (i.e., 257.7, 268, 282.3, and 301.2 nm) using UV-LEDs as light sources. The molar absorption coefficients and quantum yields of both HOCl and OCl^- at the four wavelengths were obtained, and used to establish an empirical model to predict the fluence-based chlorine photodecay rates at wavelength from 257.7 to 301.2 nm and pHs from 5 to 10. The model was then validated against the experimental results at the four wavelengths and pHs 6 and 7. The wavelength dependency on the formation of reactive radical species from chlorine photolysis at the four wavelengths and two pHs (i.e., pHs 6 and 7) were also studied.

2. Materials and methods

2.1. Chemicals and materials

Reagent-grade chemicals, including sodium hypochlorite solution (4.0–5.0%), sodium sulfite, sodium hydrogen phosphate, sodium dihydrogen phosphate, sodium bicarbonate, sodium borate, nitrobenzene (NB), and carbamazepine (CBZ) were purchased from Sigma Aldrich and used without further purification. Their stock solutions were prepared using deionized water (18.2 MΩ cm) prepared by a Nanopure water system (Barnstead).

2.2. UV exposure

UV exposure was carried out using quasi-collimated UV-LED devices (PearlBeam, AquiSense Technologies) that allow selection of one monochromatic light from four wavelengths at 257.7 (255), 268 (265), 282.3 (285), and 301.2 (300) nm, and their emission spectra are shown in Fig. 1. The values in the brackets are provided by the manufacture, which are close to the real peak emission wavelengths. Figure S2 shows the schematic of the UV-LED setup, where a rapid-mixed batch glass reactor (5 mL) containing reacting solution (~1.0 cm in depth) was placed below the LED source, and covered with a quartz sheet to prevent evaporation. The distance of the UV-LEDs to the solution surface was 7.05 cm. The incident fluence rates (E_0) of the UV-LEDs were measured at the surface of the reaction solution using a radiometer (ILT 2400) with a detector (SED 270, typically designed for UV-LEDs with emission spectral range of 215–355 nm), which was supplied by the International Light Technology and calibrated using a conventional potassium

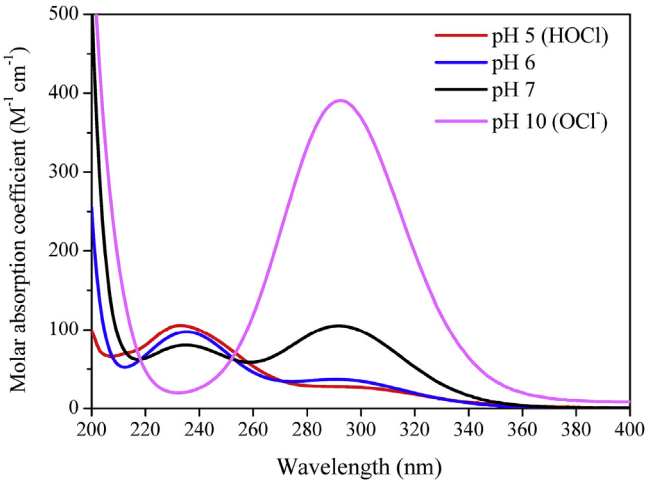

Fig. 1. The absorption spectra of free chlorine at pHs 5, 6, 7 and 10.

ferrioxalate actinometer. The values measured by the radiometer represent the integrated fluence rates under the emission spectra of the UV-LEDs and are shown in Table S1.

2.3. Experimental procedures

A testing solution of 5-mL was buffered at a particular pH (5-mM phosphate or borate buffer), spiked with a NaOCl stock solution to give an initial chlorine concentration of 100 μM (7.1 mg L^{-1} as Cl_2), and then exposed to monochromatic UV-LED light at one of the four wavelengths each time. The pH values remained the same before and after the reactions. Neither phosphate nor borate has significantly impacts on the HO· or reactive chlorine species concentrations (Buxton and Subhani, 1972; Wang et al., 2016). Carbonate/bicarbonate did not affects the concentrations of HO·, ClO· or $Cl_2^{\cdot-}$, but it may react with Cl· to form carbonate radicals, which will not contribute the degradation of probe compounds (Wu et al., 2017; Guo et al., 2017). Samples were collected at pre-determined time intervals and subjected to the measurement of residual chlorine concentrations. Tests were also conducted in a similar manner with 10-μM CBZ and NB coexisting as probing compounds to investigate the wavelength-dependency on radical generation. Samples were collected, quenched with freshly prepared sodium sulfite at a sulfite-to-chlorine molar ratio of 1.5:1, and subjected to the determination of remaining CBZ and NB concentrations.

2.4. Analytical methods

The concentrations of free chlorine were determined by the DPD colorimetric method (APHA-AWWA-WEF, 1998). The concentrations of NB and CBZ were determined using an ultra-performance liquid chromatograph (UPLC) (VP series, Shimadzu) equipped with a Waters symmetry C18 column and a UV–Vis detector. Eluents of water (pH 3, adjusted using phosphoric acid) and methanol (55:45, v/v %) were used to separate the NB and CBZ at a flow rate of 1.0 mL/min. The UV–Vis absorption spectra of chlorine-containing solutions at different pHs were measured using a UV–Vis spectrophotometer (Lambda 25, Perkin Elmer Inc., USA) with a quartz cuvette providing a light path of 1 cm.

2.5. Calculation of apparent quantum yields

The apparent quantum yields, which are defined as the number of moles of reactant consumed or product formed per einstein of photons absorbed, are calculated from the fluence-based reaction rate constants (i.e., pseudo first-order rate constants normalized by the fluence rate) (Watts and Linden, 2007):

$$k'_{(\lambda,pH)} = \frac{1}{F}\ln\left(\frac{C_0}{C_F}\right) \quad (1)$$

$$F = E_0(PF)(RF)t \quad (2)$$

$$\Phi_{(\lambda,pH)} = \frac{10k'_{(\lambda,pH)}U_\lambda}{ln(10)\varepsilon_{(\lambda,pH)}} \quad (3)$$

where $\Phi_{(\lambda,pH)}$ is the apparent quantum yield of chlorine; $k'_{(\lambda,pH)}$ is the fluence-based first-order rate constant ($m^2\ J^{-1}$); $\varepsilon_{(\lambda,pH)}$ is the molar absorption coefficient ($M^{-1}\ cm^{-1}$) of chlorine at a particular wavelength; C_0 and C_F are the initial and final concentrations of free chlorine, respectively; F is the fluence ($J\ m^{-2}$); E_0 is the incident fluence rate ($W\ m^{-2}$); PF is the petri dish factor and RF is the reflection factor; U_λ is the molar photon energy ($J\ einstein^{-1}$) of the UV light at a particular wavelength (Table S1). It should be noted that the apparent quantum yields reported in this study are the reaction quantum yields (or named overall quantum yields) of chlorine photolysis (Stefan, 2017).

2.6. Statistical analysis

The correlations between (a) chlorine photodecay rates and molar absorption coefficients and (b) chlorine photodecay rates and apparent quantum yields were evaluated by Spearman equations on Origin 8.0 software. A Spearman correlation coefficient (p value) of 1 or -1 represents that the selected two tested parameters are perfectly positive or negative monotonic functions to each other, respectively. A linear correlation function was used to examine the dependency of chlorine photodecay rates on molar absorption coefficients and quantum yields by SPSS version 19.0 (SPSS, Inc., USA), and higher standardized coefficients (β) indicate a greater effect of the independent variables have on the dependent variable. The mathematical model was constructed by Matlab (MathWorks), and the codes are shown in Text S1.

3. Results and discussion

3.1. Chlorine photodecay rates and their dependency on molar absorption coefficients

Fig. 2 shows the fluence-based rate constants of chlorine photodecay at the four wavelengths (i.e., 257.7, 268, 282.3 and 301.2 nm) and two pHs (i.e., 5 and 10). These two pHs are used to obtain the dominant (over 99%) species of HOCl and OCl^-, respectively, because HOCl has an acid dissociation constant (pK_a) of 7.5 (Morris, 1966). At pH 5, the fluence-based rate constants at 257.7, 268, 282.3 and 301.2 nm were 2.83×10^{-5}, 1.76×10^{-5}, 1.42×10^{-5}, and $1.41 \times 10^{-5}\ m^2\ J^{-1}$, respectively. The fluence-based rate constants of HOCl photodecay (k_{HOCl}) decrease by 49.8% with increasing wavelength from 257.7 to 282.3 nm, and the value at 301.2 nm is comparable to that at 283.2 nm. On the contrary, at pH 10, the fluence-based rate constants of OCl^- photodecay (k_{OCl^-}) increase with increasing wavelength from 257.7 to 301.2 nm (4.13×10^{-5}, 8.77×10^{-5}, 1.36×10^{-4}, and $1.41 \times 10^{-4}\ m^2\ J^{-1}$ at 257.7, 268, 282.3 and 301.2 nm, respectively) and increase by 3.4 times with increasing wavelength from 257.7 to 301.2 nm. The longer wavelength is found to be more efficient for chlorine

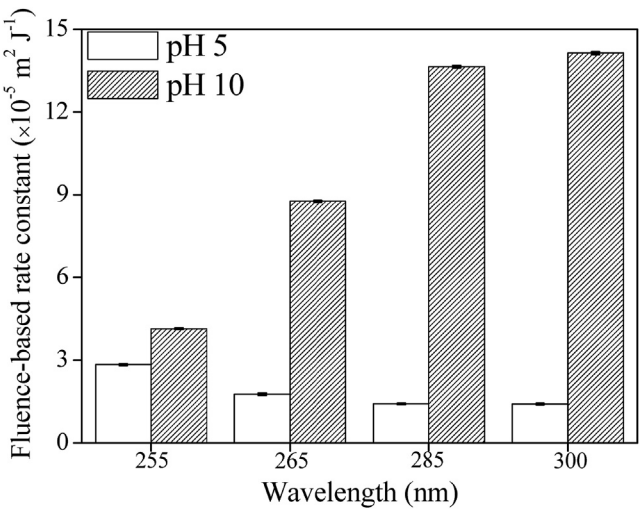

Fig. 2. Fluence-based rate constants of chlorine photodecay at the four wavelengths and two pHs. Conditions: $[Cl_2]_0 = 100$ μM (7.1 mg L^{-1} as Cl_2), pH = 5 and 10.

photodecay at pH 10, though the UV light at shorter wavelengths is considered to have higher energy.

According to the Grotthuss-Draper law, we anticipated that the observed wavelength-dependent photodecay rates were partially attributed to the light absorption of the chlorine containing solution (e.g., HOCl and OCl^-) (Turro, 1965; Wu et al., 2017). Table 1 shows the molar absorption coefficients (ε_λ) of HOCl and OCl^-, which are obtained from the absorption spectra (Figure S3). With the increasing wavelength of UV-LED from 257.7 to 301.2 nm, ε_{HOCl} decreases from 48.35 ± 1.22 to $25.21 \pm 0.90\ M^{-1}\ cm^{-1}$, while ε_{OCl-} increases from $83.32 \pm 1.07\ M^{-1}\ cm^{-1}$ to 316.35 ± 1.12. ε_{HOCl} and ε_{OCl-} are both positively correlated with the fluence-based rate constants of HOCl and OCl^-, respectively ($p_1 = p_2 = 1$, Figure S4), supporting that the wavelength-dependency on the chlorine photodecay is partially attributed to the wavelength-dependent ε_{HOCl} and ε_{OCl-}.

3.2. Dependency of chlorine photodecay rates on apparent quantum yields

Table 2 shows the apparent quantum yields of chlorine photodecay at the four wavelengths and pHs 5 and 10 calculated using Eqs. (1)–(3). At pH 5, the apparent quantum yields of HOCl photodecay were 1.18 ± 0.01, 1.11 ± 0.03, 0.98 ± 0.02, and 0.96 ± 0.03 mol einstein^{-1} at 257.7, 268, 282.3 and 301.2 nm, respectively, and decreased by 18.6% with increasing wavelength from 257.7 to 301.2 nm. At pH 10, the apparent quantum yields of OCl^- photodecay were 1.00 ± 0.03, 0.97 ± 0.01, 0.82 ± 0.02, and 0.77 ± 0.03 mol einstein^{-1} at 257.7, 268, 282.3 and 301.2 nm, respectively, and decreased by 23.0% with increasing wavelength from 257.7 to 301.2 nm. No apparent quantum yields of HOCl and OCl^- at the tested four wavelengths have been reported in the literature, while the decreasing tendency in quantum yields with increasing wavelengths is similar to that of the HOCl/OCl^- photodecay at 240, 253.7 and 280.4 nm using xenon-mercury lamps (Cooper et al., 2007). The apparent quantum yields of HOCl are positively correlated with the fluence-based rate constants ($p_4 = 1$, Figure S5), suggesting that the wavelength-dependency on the HOCl photodecay was partially attributed to the wavelength-dependent apparent quantum yields. Nevertheless, the apparent quantum yields of OCl^- are negatively correlated with the fluence-based rate constants ($p_5 = -1$, Figure S5), indicating that it was the molar absorption coefficient, but not the apparent quantum yield, resulted in the wavelength-dependency on OCl^- photodecay.

A more quantitative analysis of the dependency of $k'_{(\lambda,\ pH)}$ on $\varepsilon_{(\lambda,\ pH)}$ and $\Phi_{(\lambda,\ pH)}$ at the four wavelengths and pHs 5 and 10 was conducted using the linear correlation function in SPSS (Table S2). The standardized coefficient (β) between k'_λ and the ε_λ ($\beta_{k'_\lambda - \varepsilon\lambda} = 0.949$) is 17 times higher than that between k'_λ and Φ_λ ($\beta_{k'_\lambda - \Phi_\lambda} = 0.055$) considering all eight conditions at the four wavelengths and pHs 5 and 10, further proving that the molar absorption coefficient, instead of the apparent quantum yield, is the major contributor to the wavelength-dependent fluence-based chlorine photodecay rate constants at the tested wavelengths and pHs.

Supplementary tests were conducted to determine the photodecay rates of HOCl and OCl^- in the presence of acetate (5 mM, whose concentration is 50 times as high as that of the free chlorine), to differentiate the quantum yields of the chlorine photodecay by the direct UV photolysis or subsequent radical reactions (results are shown in Figure S3). Acetate reacts rapidly with HO· ($k = 7.50 \times 10^7\ M^{-1}\ s^{-1}$) and Cl· ($k = 3.7 \times 10^9\ M^{-1}\ s^{-1}$) without absorbing UV light at the tested wavelengths. More importantly, both acetate and its daughter radicals generated from the reactions between acetate and HO· and Cl· react slowly with free chlorine (HOCl or OCl^-) (Chuang et al., 2017). In the presence of acetate, the calculated quantum yields of the HOCl and OCl^- photodecay decreased at all tested wavelengths (Table 2), but the decrease of the calculated quantum yields of the HOCl photodecay is more significant than that of the OCl^- photodecay. The calculated quantum yields of the HOCl photodecay does not change significantly with increasing HOCl concentrations (3.55–14.2 mg L^{-1} as Cl_2, Figure S4a), but that of the OCl^- photodecay decreases significantly with increasing OCl^- concentrations (3.55–14.2 mg L^{-1} as Cl_2, Figure S4b). The results indicate that the radical scavenging by acetate can isolate the innate quantum yields of the HOCl photodecay, but is not effective for the OCl^- photodecay, probably due to the 25-fold lower reaction rate between HO· and acetate ($7.50 \times 10^7\ M^{-1}\ s^{-1}$) than that between HO· and OCl^- ($1.85 \times 10^9\ M^{-1}\ s^{-1}$) (Chuang et al., 2017). The true quantum yields of HOCl and OCl^- photodecay at 257 nm obtained in this study were 1.13 and 1.18 times as high as those reported by Chuang et al. (2017), which was probably due to the incomplete radical scavenging of HO· by acetate, because the second order rate constant between HO· and acetate ($k = 7.50 \times 10^7\ M^{-1}\ s^{-1}$) is lower than those between HOCl ($k = 5 \times 10^8\ M^{-1}\ s^{-1}$) and OCl^- ($k = 1.9 \times 10^9\ M^{-1}\ s^{-1}$), resulting in the residual radicals contributing to the decomposition of HOCl and OCl^- (Chuang et al., 2017). Moreover, it is speculated that the acetate daughter radicals still partially contributed to the free chlorine decomposition (especially for HOCl) and resulted in the overestimation of the quantum yields of chlorine photodecay, compared to the values reported by Chuang et al. (2017) by mathematical modelling ($\phi_{HOCl} = 0.62$ and $\phi_{OCl^-} = 0.55$). The differences between the apparent and true quantum yields indicated that the direct UV photolysis (reactions with other reactive species) contributed 72.0% (28.0%), 68.5% (31.5%), 66.3% (33.7%) and 62.5% (37.5%), respectively, to HOCl photodecay at 255, 265, 285 and 300 nm. And for OCl^-, direct UV photolysis contributed 91.0% (9.0%), 89.7% (10.3%), 93.9% (6.1%) and 93.5% (6.5%), respectively, at 255, 265, 285 and 300 nm.

Table 1
The molar absorption coefficients ($M^{-1}\ cm^{-1}$) of HOCl and OCl^- at the four tested wavelengths.

Wavelength (nm)	ε_{HOCl} (pH 5)	ε_{OCl^-} (pH 10)
257.7	48.35 ± 1.22	83.32 ± 1.07
268	30.82 ± 1.04	175.47 ± 1.05
282.3	26.69 ± 0.76	305.21 ± 0.98
301.2	25.21 ± 0.90	316.15 ± 1.12

3.3. Modelling of the chlorine photodecay rates

An empirical model that incorporated $\varepsilon_{(\lambda,\ pH)}$, $\Phi_{(\lambda,\ pH)}$ and U_λ was then established to predict the $k'_{(\lambda,\ pH)}$ at wavelengths from 257.7 to 301.2 nm and pHs from 5 to 10 using Eq. (4) and Matlab:

$$k'_{(\lambda,\ pH)} = \frac{ln(10)\Phi_{(\lambda,\ pH)}\varepsilon_{(\lambda,pH)}}{10U_\lambda} \tag{4}$$

where $U_\lambda = \frac{hcN_A}{\lambda}$, and h is the Planck constant ($6.6{,}260{,}690 \times 10^{-34}$ J s), c is the speed of light ($2.9{,}972{,}458 \times 10^8$ m s^{-1}), N_A is the Avogadro number ($6.0221{,}418 \times 10^{23}\ mol^{-1}$) and the wavelength λ is in meters. U_λ can be described as a function of wavelength by Eq. (5).

$$U_\lambda = \frac{h_c N_A}{\lambda} = \frac{1.19599 \times 10^8}{\lambda} \tag{5}$$

$\varepsilon_{(\lambda,pH)}$ and $\Phi_{(\lambda,\ pH)}$ of the chlorine containing solution at a certain pH can be described by Eqs. (6) and (7) (Feng et al., 2007):

Table 2
The apparent quantum yields (mol einstein^{-1}) of HOCl and OCl$^-$ in the presence/absence of acetate (5 mM) at the four tested wavelengths.

Wavelength (nm)	Φ_{HOCl}	Φ_{OCl^-}	Φ_{HOCl} *w.* acetate	Φ_{OCl^-} *w.* acetate
257.7	1.18 ± 0.01	1.00 ± 0.03	0.85 ± 0.02	0.91 ± 0.02
268	1.11 ± 0.03	0.97 ± 0.01	0.76 ± 0.01	0.87 ± 0.02
282.3	0.98 ± 0.02	0.82 ± 0.02	0.65 ± 0.03	0.77 ± 0.01
301.2	0.96 ± 0.03	0.77 ± 0.03	0.60 ± 0.01	0.72 ± 0.03

$$\varepsilon_{(\lambda,\ pH)} = f\varepsilon_{HOCl} + (1-f)\varepsilon_{OCl^-} \quad (6)$$

$$\Phi_{(\lambda,\ pH)} = \frac{f\varepsilon_{HOCl}}{f\varepsilon_{HOCl} + (1-f)\varepsilon_{OCl^-}}\Phi_{HOCl} + \frac{(1-f)\varepsilon_{OCl^-}}{f\varepsilon_{HOCl} + (1-f)\varepsilon_{OCl^-}}\Phi_{OCl^-} \quad (7)$$

f is the fraction of HOCl existing in solution at a certain pH and can be described by Eq. (8):

$$f = \frac{1}{1 + 10^{pH-7.5}} \quad (8)$$

$\varepsilon_{(\lambda,\ pH)}$ of HOCl and OCl$^-$ were measured experimentally and can be obtained from Fig. 1. The $\Phi_{(\lambda,\ pH)}$ of HOCl and OCl$^-$ at wavelengths from 257.7 to 301.2 nm were modelled empirically by fitting the experimental data (obtained from Table 2) to two equations (Fig. 3) (Cooper et al., 2007):

$$\Phi_{HOCl} = -5.2556 \times 10^{-3}\lambda + 2.5149 \quad R^2 = 0.886 \quad (9)$$

$$\Phi_{OCl^-} = -5.7346 \times 10^{-3}\lambda + 2.4802 \quad R^2 = 0.928 \quad (10)$$

The incorporated model was validated against the experimental results of chlorine photodecay at the four tested wavelengths (i.e., 257.7, 268, 282.3, and 301.2 nm) and three environmentally relevant pHs (i.e., pHs 6, 7 and 8). As shown in Fig. 4, the predicted fluence-based rate constants of chlorine photodecay (shown by the lines) are in reasonable good agreement with the experimental results (shown by the dots) at pHs 6, 7 and 8 (the difference is within 10%).

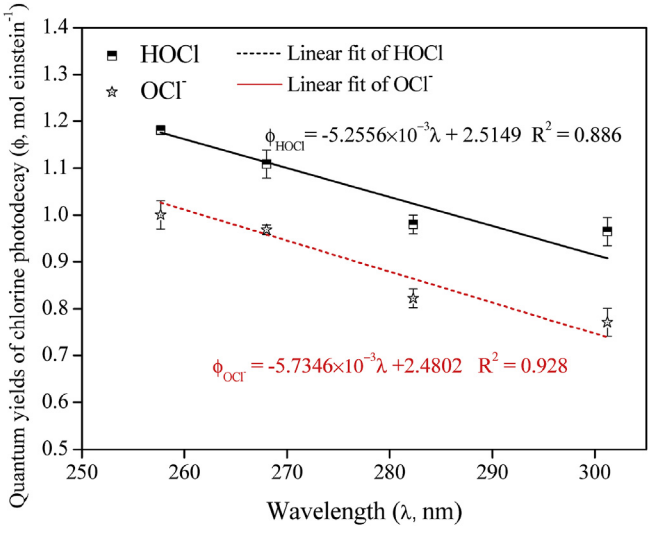

Fig. 3. Correlation between apparent quantum yields of HOCl and OCl$^-$ photodeacay and wavelengths. Conditions: $[Cl_2]_0 = 100\ \mu M$ (7.1 mg L^{-1} as Cl_2).

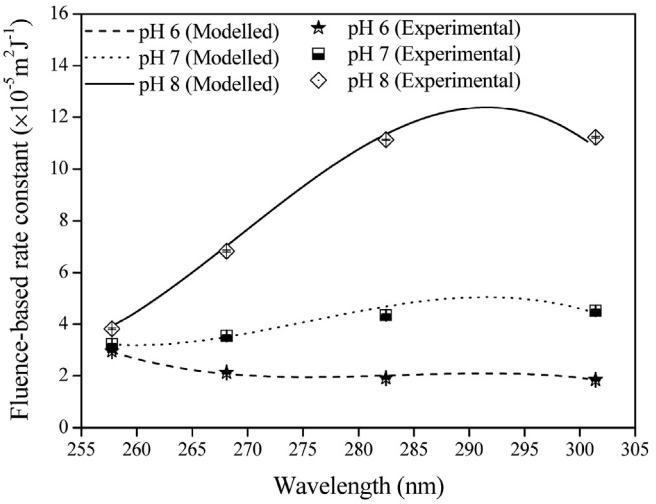

Fig. 4. Comparison between the modelled and experimental results of the fluence-based rate constants of chlorine photodecay at the four wavelengths and three pHs. $[Cl_2]_0 = 100\ \mu M$ (7.1 mg L^{-1} as Cl_2), pH = 6, 7 and 8.

Fig. 5 displays the modelling results of the wavelength- and pH-dependency on the chlorine photodecay rate. The wavelength dependency is larger at alkaline pH than at acidic pH, and the largest wavelength dependency occurs at the highest pH. As for the pH dependency, the chlorine photodecay rate constants increase with increasing pHs at any wavelength, and the pH dependency is the largest at the longest wavelength. Moreover, the maximum fluence-based rate constant (1.41×10^{-4} m^2 J^{-1}) obtained from the model is at 292 nm and pH 9.95, and the minimum (1.09×10^{-5} m^2 J^{-1}) is obtained at 291 nm and pH 5. The results verify our hypothesis that the maximum photolysis rate is obtained

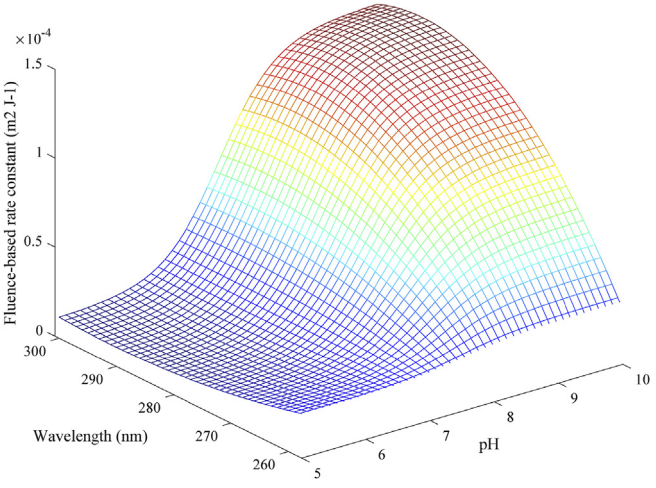

Fig. 5. Modelled results of the fluence-based rate constant of chlorine photodecay versus wavelength and pH.

near the maximum absorption of the oxidant precursor, OCl^-, which has a maximum absorption at 292 nm (Feng et al., 2007).

3.4. Wavelength- and pH-dependency on radical formation from chlorine photolysis

Nitrobenzene (NB) and carbamazepine (CBZ) were used as probes to quantify the HO· and reactive chlorine species (RCS) generated from the chlorine photolysis at the four tested wavelengths (i.e., 257.7, 268, 282.3, and 301.2 nm) and three environmentally relevant pHs (i.e., pHs 6, 7 and 8). NB exhibits high reactivity towards HO· ($k = 3.9 \times 10^9\ M^{-1}\ s^{-1}$) but hardly reacts with RCS (Buxton and Subhani, 1972; Fang et al., 2014). CBZ reacts rapidly with HO· ($k = 8.8 \times 10^9\ M^{-1}\ s^{-1}$), Cl· ($k = 5.6 \times 10^{10}\ M^{-1}\ s^{-1}$) (Wang et al., 2016) and ClO· ($0.92 \times 10^8\ M^{-1}\ s^{-1}$) (Guo et al., 2017). Also, it has been reported in the literature that the steady-state concentrations of Cl·, ClO· and $Cl_2^{\cdot-}$ are in the order of 10^{-14}, 10^{-10}, and 10^{-14} M in the UV/chlorine process under the environmentally relevant conditions similar to the current study (Guo et al., 2017). Based on the information on the rate constants and the concentrations of the radical species, the contribution of ClO· to CBZ degradation in the UV/chlorine process is thus around 2 magnitudes higher than that of Cl·, and much higher than that of $Cl_2^{\cdot-}$. Therefore, ClO· was selected as the representative RCS and its second order rate constant was used to calculate the steady-state concentration of RCS in this study (such assumption may cause the overestimation of the steady-state concentrations of ClO·, and it was only recommended to be used to compare the wavelength- and pH-dependency on radical formation in this study). In addition, it should be noted that both NB and CBZ are inert to direct UV-LED photolysis and dark chlorination in the time scale of the current study (less than 5%, as shown Figure S7). Therefore, the NB and CBZ degradation can be expressed by Eqs. (11) and (12):

$$-\frac{dC_{NB}}{dt} = k_{HO\cdot-NB}[HO\cdot]_{ss}C_{NB} = k_{O,NB}C_{NB} \tag{11}$$

$$-\frac{dC_{CBZ}}{dt} = k_{HO\cdot-CBZ}[HO\cdot]_{ss}C_{CBZ} + k_{ClO\cdot-CBZ}[ClO\cdot]_{ss}C_{CBZ} = k_{O,CBZ}C_{CBZ} \tag{12}$$

where $k_{HO\cdot-NB}$ and $k_{HO\cdot-CBZ}$ are the second-order rate constants of HO• towards NB ($k = 3.9 \times 10^9\ M^{-1}\ s^{-1}$) and CBZ ($k = 8.8 \times 10^9\ M^{-1}\ s^{-1}$), respectively; and $k_{ClO\cdot-CBZ}$ is the second-order rate constant of ClO· towards CBZ ($k = 0.92 \times 10^8\ M^{-1}\ s^{-1}$); $k_{O,NB}$ and $k_{O,CBZ}$ are the apparent pseudo first-order rate constants of the NB and CBZ degradation (shown in Figures S8 and S9), respectively. $[HO\bullet]_{ss}$ and $[ClO\bullet]_{ss}$ are the steady-state concentrations of HO· and ClO·, respectively.

The steady-state concentrations of HO·($[HO\cdot]_{ss}$) and ClO·($[ClO\cdot]_{ss}$) were thus obtained and normalized with the fluence rates and are shown in Fig. 6 (un-normalized data are shown in Figure S10). At pH 6, the fluence-based $[HO\cdot]_{ss}$ decreased from 1.8×10^{-14} to 1.2×10^{-14} $(W/m^2)^{-1}\ M^{-1}$ with increasing wavelength from 257.7 to 301.2 nm, which decreased by 32.03%. $[ClO\cdot]_{ss}$ decreased also, by 57.95% (from 9.6×10^{-13} to 4.0×10^{-13} $(W/m^2)^{-1}\ M^{-1}$), with increasing wavelength from 257.7 to 301.2 nm. Compared to HO·, ClO· decreased more significantly with increasing the wavelength from 257.7 to 301.2 nm at pH 6. Nonetheless, at pHs 7, the fluence-based $[HO\cdot]_{ss}$ increased from 9.1×10^{-15} to 1.2×10^{-14} $(W/m^2)^{-1}\ M^{-1}$ with increasing wavelength from 257.7 to 301.2 nm, which increased by 30.43%. And the $[ClO\cdot]_{ss}$ also increased by 32.80%, from 1.2×10^{-12} to 1.7×10^{-12} $(W/m^2)^{-1}\ M^{-1}$, with increasing wavelength from 257.7 to 301.2 nm. At pH 8, the fluence-based $[HO\cdot]_{ss}$ and $[ClO\cdot]_{ss}$ increased by 57.02% and 58.39%, respectively, with increasing wavelength from 257.7 to 301.2 nm. Compared to the fluence-based $[HO\cdot]_{ss}$, that of ClO· increased more significantly with increasing wavelengths from 257.7 to 301.2 nm at pHs 7 and 8. These findings indicate that the formation of ClO· is more wavelength-dependent than that of HO·. And the impact of wavelength on the HO· and ClO· formation was more significant at pH 6, compared to those at pHs 7 and 8. Fig. 5 also shows that, at any wavelength tested, the fluence-based $[HO\cdot]_{ss}$ decrease with increasing pHs, mainly due to the faster scavenging rate of HO· by OCl^- ($k = 8.8 \times 10^9\ M^{-1}\ s^{-1}$) than that by HOCl ($k = 2.0 \times 10^9\ M^{-1}\ s^{-1}$) and the higher OCl^- concentration at higher pHs (Fang et al., 2014). In contrast, the fluence-based $[ClO\cdot]_{ss}$ increase with increasing pHs, at any wavelength tested, due to the weaker scavenging effect of OCl-than HOCl towards ClO· and the increasing formation of ClO· from the scavenging of HO· by OCl^- at higher pHs (Guo et al., 2017). At higher pHs, the formation of higher $[ClO\cdot]_{ss}$ offset the scavenging of HO· for the CBZ degradation in the process, resulting in the higher apparent rate constants of the CBZ degradation. In addition, the fluence-based $[HO\cdot]_{ss}$ and $[ClO\cdot]_{ss}$

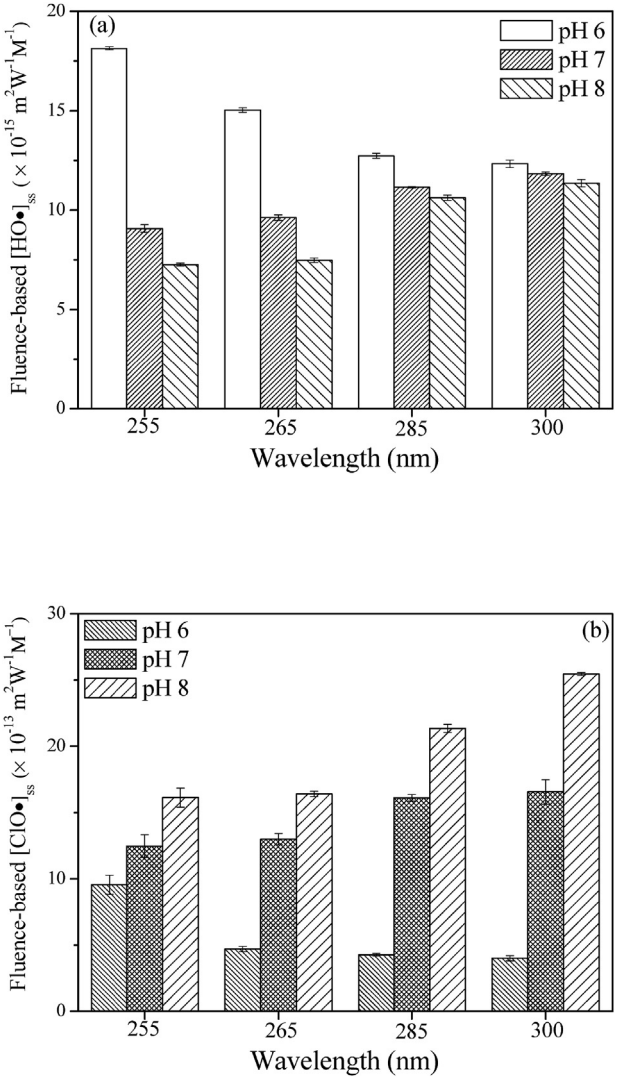

Fig. 6. The fluence-based steady-state concentrations of (a) HO• and (b) ClO• at the four wavelengths and three pHs. $[Cl_2]_0 = 100\ \mu M$ (7.1 mg L^{-1} as Cl_2), $[CBZ]_0 = [NB]_0 = 10\ \mu M$, pH = 6, 7 and 8.

show positive correlation ($p_6 = p_7 = p_8 = p_9 = 1$) with the fluence-based rate constants of chlorine photodecay (Figure S11), indicating that the radical formation exhibited a similar wavelength-dependency to the chlorine photodecay. The wavelength- and pH-dependency on the formation of other RCS (e.g., Cl· and $Cl_2^{\cdot-}$), and the relationship between the radical yield and the chlorine photodecay will be further investigated in the future.

4. Conclusions

The photodecay rates of HOCl and OCl^- were highly wavelength-dependent, mainly due to the wavelength-dependent molar absorption coefficients, instead of quantum yields. As predicted by the empirical model, the wavelength dependency is larger at alkaline pH than at acidic pH and the largest wavelength dependency occurs at the highest pH. As for the pH dependency, the chlorine photodecay rate constants all increase with increasing pH at any wavelength, and the pH dependency is the largest at the longest wavelength.

The modelled results help us better select UV-LEDs at different wavelengths for chlorine photodecay and micropollutant degradation by the UV/chlorine AOP, based on the pH condition of the target water. UV light at longer wavelength is more suitable for photo-dechlorination of chlorine in swimming pools and pollutant degradation by the UV/chlorine AOP in water (e.g., secondary effluents and surface water) at neutral and alkaline pH. The wall plug efficiency of UV-LED at high wavelength (e.g., 301.2 nm) is predicted to reach 75% by 2020 (Song et al., 2016), which makes it a promising alternative to the conventional UV mercury lamps for chlorine photodecay and micro-pollutant degradation by the UV/chlorine AOP in the near future at neutral and alkaline pH. On the other hand, the UV light at shorter wavelength is more suitable for the chlorine photodecay and micropollutant degradation by the UV/chlorine AOP in water at acidic pH (e.g., <6.5). In these cases, conventional UV mercury lamps still perform better than UV-LED at low wavelength (e.g., 257.7 nm), since the wall plug efficiency of UV-LED at 257.7 nm will unlikely be significantly improved enough to compete with the conventional lamps in the foreseeable future.

Acknowledgements

This work was supported by the Hong Kong Research Grants Council (grant number 16202217). The authors also want to thank Mr. Ping Shen for his suggestions on the Matlab programming.

Appendix A. Supplementary data

Supplementary data related to this article can be found at https://doi.org/10.1016/j.watres.2018.06.018.

References

APHA-AWWA-WEF, 1998. Standard methods for the examination of water and wastewater. In: American Public Health Association/American Water Works Association/Water Environment Federation, Washington DC, US, twentieth ed.
Buxton, G., Subhani, M., 1972. Radiation chemistry and photochemistry of oxychlorine ions. Part 1.—radiolysis of aqueous solutions of hypochlorite and chlorite ions. J. Chem. Soc. Farad. Trans. 1 Phys.Chem. Conden. Phas. 68, 947–957.
Buxton, G.V., Greenstock, C.L., Helman, W.P., Ross, A.B., 1988. Critical review of rate constants for reactions of hydrated electrons, hydrogen atoms and hydroxyl radicals (·OH/·O⁻) in aqueous solution. J. Phys. Chem. Ref. Data 17 (2), 513–886.
Cassan, D., Mercier, B., Castex, F., Rambaud, A., 2006. Effects of medium-pressure UV lamps radiation on water quality in a chlorinated indoor swimming pool. Chemosphere 62 (9), 1507–1513.
Chen, J., Loeb, S., Kim, J.H., 2017. LED revolution: fundamentals and prospects for UV disinfection applications. Environ. Sci. Water Res. Technol. 3 (2), 188–202.
Chuang, Y.H., Chen, S., Chinn, C.J., Mitch, W.A., 2017. Comparing the UV/monochloramine and UV/free chlorine advanced oxidation processes (AOPs) to the UV/hydrogen peroxide AOP under scenarios relevant to potable reuse. Environ. Sci. Technol. 51 (23), 13859–13868.
Cooper, W.J., Jones, A.C., Whitehead, R.F., Zika, R.G., 2007. Sunlight-induced photochemical decay of oxidants in natural waters: implications in ballast water treatment. Environ. Sci. Technol. 41 (10), 3728–3733.
Deng, L., Huang, C.H., Wang, Y.L., 2014. Effects of combined UV and chlorine treatment on the formation of trichloronitromethane from amine precursors. Environ. Sci. Technol. 48 (5), 2697–2705.
Dotson, A., Rodriguez, C.E., Linden, K.G., 2012. UV disinfection implementation status in US water treatment plants. J. Am. Water Works Assoc. 104 (5), 77–78.
Fang, J., Fu, Y., Shang, C., 2014. The roles of reactive species in micropollutant degradation in the UV/free chlorine system. Environ. Sci. Technol. 48 (3), 1859–1868.
Feng, Y., Smith, D.W., Bolton, J.R., 2007. Photolysis of aqueous free chlorine species (HOCl and OCl^-) with 254 nm ultraviolet light. J. Environ. Eng. Sci. 6 (3), 277–284.
Forsyth, J.E., Zhou, P., Mao, Q., Asato, S.S., Meschke, J.S., Dodd, M.C., 2013. Enhanced inactivation of Bacillus subtilis spores during solar photolysis of free available chlorine. Environ. Sci. Technol. 47 (22), 12976–12984.
Guo, K., Wu, Z., Shang, C., Yao, B., Hou, S., Yang, X., Song, W., Fang, J., 2017. Radical chemistry and structural relationships of PPCP degradation by UV/chlorine treatment in simulated drinking water. Environ. Sci. Technol. 51 (18), 10431–10439.
He, X., Pelaez, M., Westrick, J.A., O'Shea, K.E., Hiskia, A., Triantis, T., Kaloudis, T., Stefan, M.I., Armah, A., Dionysiou, D.D., 2012. Efficient removal of microcystin-LR by UV-C/H_2O_2 in synthetic and natural water samples. Water Res. 46 (5), 1501–1510.
Jin, J., El-Din, M.G., Bolton, J.R., 2011. Assessment of the UV/chlorine process as an advanced oxidation process. Water Res. 45 (4), 1890–1896.
Kashinkunti, R.D., Linden, K.G., Shin, G.-A., Metz, D.H., Sobsey, M.D., Moran, M.C., Samuelson, A.M., 2004. Investigating multibarrier inactivation for Cincinnati—UV, by-products, and biostability. J. Am. Water Works Assoc. 96 (6), 114–127.
Muramoto, Y., Kimura, M., Nouda, S., 2014. Development and future of ultraviolet light-emitting diodes: UV-LED will replace the UV lamp. Semicond. Sci. Technol. 29 (8), 084004.
Morris, J.C., 1966. The acid ionization constant of HOCl from 5 to 35. J. Phys. Chem. 70 (12), 3798–3805.
Örmeci, B., Linden, K.G., Ducoste, J.J., 2005. UV disinfection of chlorinated water: impact on chlorine concentration and UV dose delivery. J. Water Supply Res. Technol. - Aqua 54 (3), 189–199.
Remucal, C., Manley, D., 2016. Emerging investigators series: the efficacy of chlorine photolysis as an advanced oxidation process for drinking water treatment. Environ. Sci. Water Res. Technol. 2 (4), 565–579.
Rosenfeldt, E.J., Linden, K.G., 2007. The R_{OH}, UV concept to characterize and the model UV/H_2O_2 process in natural waters. Environ. Sci. Technol. 41 (7), 2548–2553.
Song, K., Mohseni, M., Taghipour, F., 2016. Application of ultraviolet light-emitting diodes (UV-LEDs) for water disinfection: a review. Water Res. 94, 341–349.
Sun, P., Lee, W.N., Zhang, R., Huang, C.H., 2016. Degradation of DEET and caffeine under UV/chlorine and simulated sunlight/chlorine conditions. Environ. Sci. Technol. 50 (24), 13265–13273.
Stefan, M.I. (Ed.), 2017. Advanced Oxidation Processes for Water Treatment: Fundamentals and Applications. IWA publishing.
Turro, N.J., 1965. Modern Molecular Photochemistry. University Science Books, Sausalito, California.
Wang, G.S., Hsieh, S.T., Hong, C.S., 2000. Destruction of humic acid in water by UV light-catalyzed oxidation with hydrogen peroxide. Water Res. 34 (15), 3882–3887.
Wang, W.L., Wu, Q.Y., Huang, N., Wang, T., Hu, H.Y., 2016. Synergistic effect between UV and chlorine (UV/chlorine) on the degradation of carbamazepine: influence factors and radical species. Water Res. 98, 190–198.
Watts, M.J., Linden, K.G., 2007. Chlorine photolysis and subsequent OH radical production during UV treatment of chlorinated water. Water Res. 41 (13), 2871–2878.
Weng, S., Li, J., Blatchley, E.R., 2012. Effects of UV_{254} irradiation on residual chlorine and DBPs in chlorination of model organic-N precursors in swimming pools. Water Res. 46 (8), 2674–2682.
Wu, B., Yang, M., Yin, R., Zhang, S., 2017. Applicability of light sources and the inner filter effect in UV/acetylacetone and UV/H_2O_2 processes. J. Hazard Mater. 335, 100–107.
Würtele, M., Kolbe, T., Lipsz, M., Külberg, A., Weyers, M., Kneissl, M., Jekel, M., 2011. Application of GaN-based ultraviolet-C light emitting diodes (UV LEDs) for water disinfection. Water Res. 45 (3), 1481–1489.
Yang, X., Sun, J., Fu, W., Shang, C., Li, Y., Chen, Y., Gan, W., Fang, J., 2016. PPCP degradation by UV/chlorine treatment and its impact on DBP formation potential in real waters. Water Res. 98, 309–318.
Yin, R., Zhong, Z., Ling, L., Shang, C., 2018. The fate of dichloroacetonitrile in the UV/Cl_2 and UV/H_2O_2 processes: implications on potable water reuse. Environ. Sci. Water Res. Technol. https://doi.org/10.1039/C8EW00195B.
Zhou, P., Di Giovanni, G.D., Meschke, J.S., Dodd, M.C., 2014. Enhanced inactivation of Cryptosporidium parvum oocysts during solar photolysis of free available chlorine. Environ. Sci. Technol. Lett. 1 (11), 453–458.